Phosphorus, Sulfur, and Silicon and the Related Elements

ISSN: (Print) (Online) Journal homepage: https://www.tandfonline.com/loi/gpss20

Reduction of phosphogypsum to calcium sulfide (CaS) using metallic iron in a hydrochloric acid medium

Majda Alla, Achraf Harrou, Mohammed Lamine Elhafiany, Dounia Azerkane, Meriam El Ouahabi & El Khadir Gharibi

To cite this article: Majda Alla, Achraf Harrou, Mohammed Lamine Elhafiany, Dounia Azerkane, Meriam El Ouahabi & El Khadir Gharibi (2022): Reduction of phosphogypsum to calcium sulfide (CaS) using metallic iron in a hydrochloric acid medium, Phosphorus, Sulfur, and Silicon and the Related Elements, DOI: 10.1080/10426507.2022.2052881

To link to this article: https://doi.org/10.1080/10426507.2022.2052881

PHOSPHORUS, SULFUR, AND SILICON AND THE RELATED ELEMENTS
https://doi.org/10.1080/10426507.2022.2052881

Reduction of phosphogypsum to calcium sulfide (CaS) using metallic iron in a hydrochloric acid medium

Majda Alla[a], Achraf Harrou[b], Mohammed Lamine Elhafiany[a], Dounia Azerkane[b], Meriam El Ouahabi[c], and El Khadir Gharibi[b]

[a]Laboratory of Electrical Engineering and maintenance, Higher School of Technology, Mohammed First University, Oujda, Morocco; [b]Laboratory of Applied Chemistry and Environment Team of Mineral Solid Chemistry, Faculty of Sciences, Mohammed First University, Oujda, Morocco; [c]UR Argile, Géochimie et Environnement sédimentaires (AGEs), Département de Géologie, University of Liège, Liège, Belgium

ABSTRACT

Our study aims to decompose phosphogypsum (PG), mainly composed of $CaSO_4.2H_2O$, by reduction in an acidic medium. We evaluated the decomposition of PG by various reaction mechanisms. Sulfate ions from the acid digestion of PG are reduced to sulfide by the hydrogen gas produced in the solution by hydrochloric attack of the metal iron. The solid residues obtained have been determined and monitored by X-Ray Diffraction, Fourier-Transform Infrared spectroscopy and Ultraviolet-visible spectroscopy. The microstructure of residues was observed by scanning electron microscope (SEM). The results show that hydrogen gas formed by hydrochloric acid attack of iron reduces the sulfur from S(VI) to S(-II). $CaSO_4.2H_2O$, insoluble in water, gives a residue containing CaS, which is only sparingly soluble in water. The residue also contains anhydrite, bassanite and ferrous chloride. The monitoring of the quantities of residue obtained under varying experimental conditions (temperature, attack time, mass of iron and PG and volume of acid on PG) and volume of HCl showed that the amounts of residue obtained are less than 32% of mass. When the volume of the HCl added increases, the obtained mass of the solid residue decreases sharply. The residue stabilizes at 10% of mass when the volume of HCl added is higher than that required to attack metal iron.

ARTICLE HISTORY
Received 14 June 2021
Accepted 9 March 2022

KEYWORDS
Phosphogypsum; CaS; hydrochloric attack; sulfur reduction; waste recycling

GRAPHICAL ABSTRACT

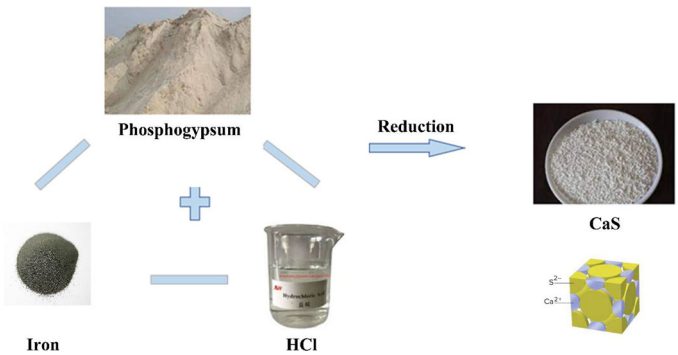

Introduction

The recovery of industrial and mining wastes, produced in large quantities as phosphogypsum (PG), is a matter of very high industrial and social importance, taking into account the principles of circular economy and environmental protection.[1] Whatever the field of application of by-products, mining waste recycling will be attractive for reduction of solid waste and conservation of finite nonrenewable natural resources.[2]

The synthesis of phosphoric acid, by the dihydrate process at a temperature ranging from 90 to 120 °C, produces P_2O_5 in amounts between 42 and 52%.[3] The synthesis of H_3PO_4 generates phosphogypsum waste, which is mainly composed of gypsum ($CaSO_4.2H_2O$). The quantity of PG produced on an industrial scale is about 5 tons for one ton of phosphoric acid.[4,5] Rock phosphate also contains fluorite and carbonates, which react with sulfuric acid and increase the content of the phosphogypsum formed.

Morocco is one of the world leaders in the production of phosphoric acid and phosphate fertilizers from phosphate rocks. It is the world's leading exporter of phosphate in all its forms, with an annual production of twelve million tons.[6] Morocco held second place among the phosphate

CONTACT El Khadir Gharibi gharibi_elkhadir@yahoo.fr Laboratory of Applied Chemistry and Environment Team of Mineral Solid Chemistry, Faculty of Sciences, Mohammed First University, Oujda 60000, Morocco.

Table 1. Labels of raw materials and formulations used for XRD analysis.

Label	Samples
E1	Raw phosphogypsum (PG).
E2	Metallic iron (Fe).
E3	PG (50%) + Fe (50%) before adding HCl.
E4	Solid residue of PG (50%) + Fe (50%) mixture after the addition of 20 mL of HCl (C = 12.06 M).
E5	Solid residue after acid attack of 20 mL of HCl (C = 12.06 M) on Fe.
E6	Solid residue after acid attack of 20 mL of HCl (C = 12.06 M) on raw PG.

exporters, with 15% of world trade, and has a natural phosphate reserve estimated at 70% and 38% in concentrate.[7–9] Its operating life is 2000 years, based on the reserve/production ratio of 2014; it has now been estimated at 370 years because of the rise in global demand.[10,11] In Morocco, the annual production of PG exceeds 20 million tons/year,[12] it is about one tenth of the world production estimated at 250 million tons/year.[3] Various recovery operations of phosphogypsum as a road backfill,[13–16] fertilizer, additive to cements and source of sulfur dioxide have been studied.[17–23] However, the presence of harmful elements such as heavy metals (Cd, Zn, Cu and Cr), radionuclides (Ra, U and Th) and fluorine limit the fields of recovery of PG.[24,25]

Phosphogypsum decomposition has been studied under various experimental conditions, such as reducing gases and reacting with different types of carbon. Thermochemical decomposition of PG to sulfur dioxide and lime provides possibilities to use its main components CaO and S and, at the same time, to solve some environmental problems.[26] Thermal decomposition of PG in air generally occurs at very high temperatures exceeding 1400 °C.[27] PG can also decompose in a reducing atmosphere, under CO for example, at a lower temperature according to the Muller-Khune process.[28–31] The SO_2 gas, produced in amounts ranging between 7 and 10%, is washed and then transported to the sulfuric acid production units.[32]

The addition of $FeCl_3$ a catalyst helped to initiate the decomposition of $CaSO_4$, under CO (g) from 700 °C to give CaS.[33]

PG can also be reduced with H_2 between 1100 and 1200 °C in a fluidized bed reactor fed with a hydrocarbon fuel and air or by combustion of natural gas.[34] $CaSO_4$ decomposes in the presence of carbon monoxide CO (g) and hydrogen H_2 (g), to give sulfur dioxide up 1150 °C.[35]

The solubility of gypsum in fresh water reaches a maximum value of 2.25 g/L from about 40 °C and decreases at lower or higher temperatures.[36] In hydrochloric acid solution (3 M HCl), the solubility of gypsum reaches 47 g/L at 80 °C.[37] Oumnih et al. [38] studied the possible reactions of PG mixed with Fe and HCl. They demonstrated that the reactions are accompanied by the release of SO_2, H_2S or H_2. The SO_2 is thermodynamically the most favorable.

Studies of reductive decomposition of phosphogypsum to SO_2 remain limited. Most published results deal with thermogravimetric analysis, which is insufficient to study the decomposition behavior of phosphogypsum to SO_2. Problems related to the control of the reaction conditions must be solved, and further insight into the theory of reductive of phosphogypsum to sulfur dioxide and lime is requested.

Calcium sulfide is very difficult to prepare in an aqueous solution due to hydrolysis, and therefore bulk CaS usually prepared in a high temperature environment (1200 °C) and requires toxic H_2S gas.[39] Above 950 °C, CaS can be obtained by reaction of SO_2 gas with CaO, but it is accompanied by $CaSO_4$ and $CaSO_3$.[40] Likewise, CaS films were coated on micro-slides by the reaction of a solution of ($CaSO_4$), ($Na_2S_2O_3.5H_2O$), distilled water, and EDTA.[41,42] Iron-doped calcium sulfide nanoparticles were synthesized by co-precipitation in ethanol of $Na_2S.9H_2O$ and ($FeCl_2.4H_2O$, $CaCl_2$).[42]

Our study is part of the sustainable management of phosphogypsum. We seek to evaluate the decomposition of PG mixed with metallic iron and HCl by combining several reaction mechanisms. By hydrochloric attack, metallic iron will release the reducing gas H_2 into the reaction medium, the latter will reduce the sulfate ions (SO_4^{2-}) resulting from the dissolution of $CaSO_4$, accelerated by HCl. Sulfur (VI), in the form of SO_4^{2-} ions in solution, is reduced by the reducing gas H_2. It can form salts with the lowest possible oxidation state. By X-ray diffraction, we will follow the evolution of insoluble solid residues. The theoretical calculation of the free enthalpies of the reactions will verify the reactions giving the salts evidenced by the XRD.

Results and discussion

Characterization of raw materials and residues

The raw materials and the treated samples used for XRD analysis are illustrated in Table 1.

The XRD results of PG, dried at 50 °C for 12 h (E1) and after attack by HCl (E6), show the occurrence of gypsum ($CaSO_4.2H_2O$), bassanite ($CaSO_4.1/2H_2O$), anhydrite ($CaSO_4$) and quartz (SiO_2) (Figure 1A).

The dried PG residue at 110 °C for 24 h obtained after attack with HCl at 50 °C for 30 min, which represents about 25% of the initial mass, consists mainly of bassanite and anhydrite identified by their characteristic peaks $2\theta = 14.70°$, 25.67° and 31.90° for bassanite and $2\theta = 25.43°$ and 31.36° for anhydrite. Quartz is not attacked by acid. HCl reacts with metallic iron allowing the formation of $FeCl_2.4H_2O$ [43] (Figure 1B).

The spectrum of the solid residue obtained by acid attack of the PG in the presence of metallic iron are illustrated in Figure 1C. The total disappearance of gypsum peaks, the presence of anhydrite, bassanite, iron chloride hydrates ($FeCl_2.4H_2O$) and the formation of calcium sulfide (CaS; JCPDS 01-075-0261) are observed. The XRD characteristic peaks of CaS (2θ = 31.4 and 45.08) clearly appear in E4 but are absent in E3.

CaS and $FeCl_2.4H_2O$ are obtained according to the following reaction:

$$CaSO_4.2H_2O + 5Fe + 10HCl + 14H_2O \rightarrow CaS + 5FeCl_2.4H_2O + H_2$$

$$\Delta H^{\circ}_{298} = -450.9\ kJ.mol^{-1},$$

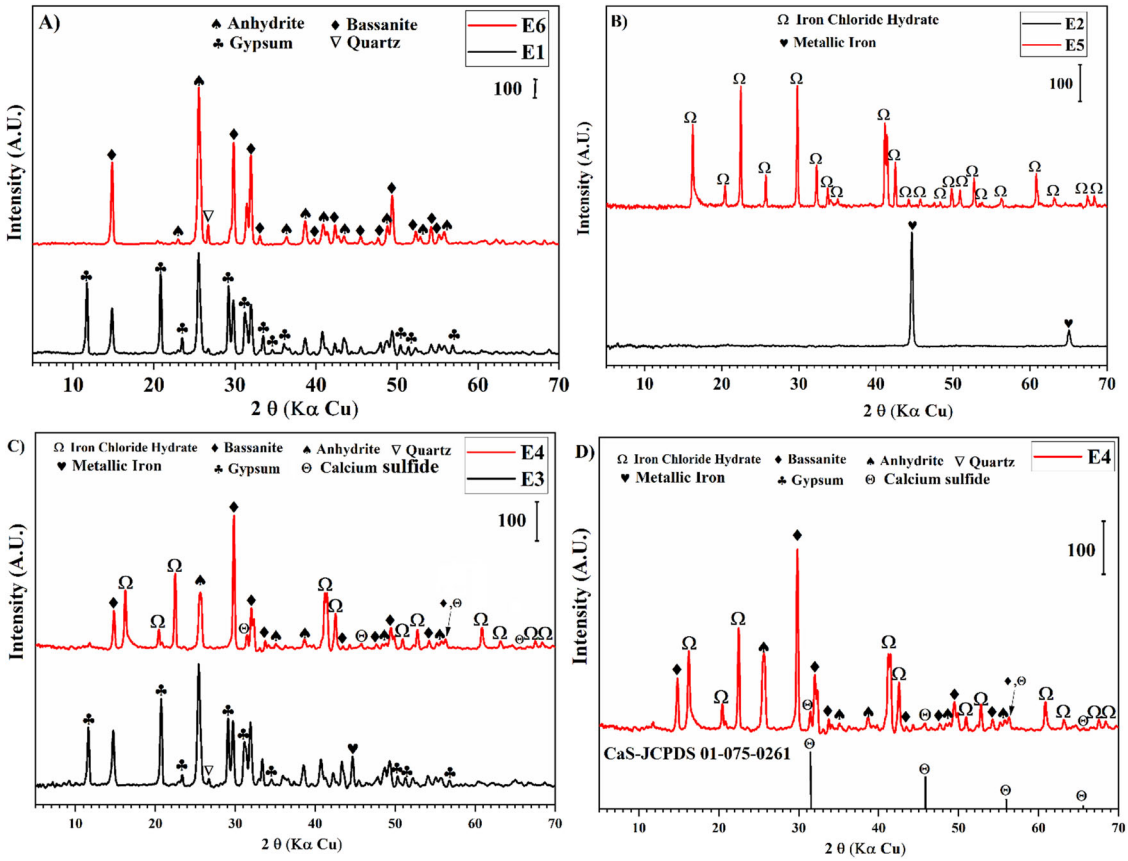

Figure 1. XRD spectra of raw materials, mixtures and solid residue. (A) raw PG (E1) and PG attacked by HCl (E6). (B) raw iron metallic (E2) and solid residue after acid attack on Fe (E5). (C) PG (50%) + Fe (50%) (E3) and solid residue of PG (50%) + Fe (50%) + HCl (E4). (D) Solid residue of PG (50%) + Fe (50%) + HCl (E4) with ICPDS card of CaS.

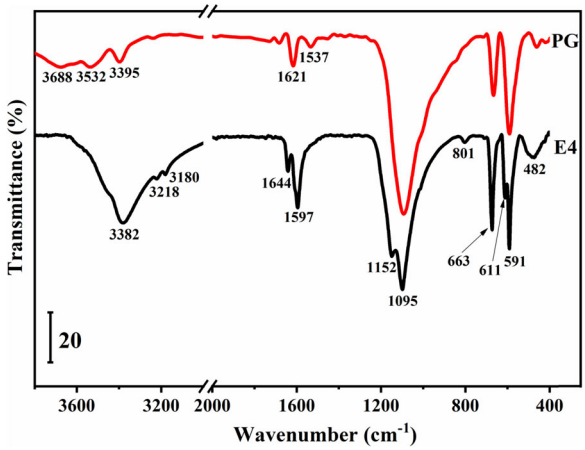

Figure 2. ATR-FTIR Spectra of raw phosphogypsum (E1) and solid residue of PG (50%) + Fe (50%) mixture after acid attack (E4).

$$\Delta G^{\circ}_{298} = -442.4\ kJ.mol^{-1}$$

This reaction is strongly exothermic and produces 23.8 L of hydrogen for one mole of $CaSO_4.2H_2O$. The specific volume of H_2 is 11.9 m^3/kg at 20 °C,[44] allowing to maintain anaerobic conditions and the stability of the sulfide.[45]

If we consider the dissolution of ferrous chloride tetrahydrate (1600 g/L), the chemical reaction becomes:

$$CaSO_4.2H_2O + 5Fe + 10HCl \rightarrow CaS + 5Fe^{2+} + 10Cl^{-} + 6H_2O + H_2$$

$$\Delta H^{\circ}_{298} = -538.1\ kJ.mol^{-1}$$

$$\Delta G^{\circ}_{298} = -591.9\ kJ.mol^{-1}$$

The insoluble solid residue represents a minimum amount of 32% of the mass of the initial solid.

Figure 2 shows the ATR-FTIR spectra of raw PG sample (E1) and solid residue of PG (50%) mixed with Fe (50%) and treated with 20 mL of HCl. The peak at 3688 cm^{-1} is due to the elongation of the O-H bond of the adsorbed water. PG shows a peak at 3390 cm^{-1} attributed to symmetrical and asymmetric elongations of the OH bond of gypsum molecule $CaSO_4.2H_2O$.[46]

The elongation and strain of the SO_4 group of the PG are observed at 1095 cm^{-1}, 663 cm^{-1} and 591 cm^{-1} respectively. Peaks due to the elongation of the symmetric and asymmetric O-H bond are observed between 1600 and 1500 cm^{-1}. A small peak at 482 cm^{-1} is due to the symmetric and asymmetric elongation of the Si-O-Si bond of quartz, present in small amount, is observed in PG.[6] The band at 611 cm^{-1} can to be assigned to the antisymmetric stretches of the S-O single bonds in the three-membered ring of the C_{2v} of the free SO_4^{2-} anion.[47,48]

The solid residue from acid attack of PG in the presence of iron shows the disappearance of the peak at 3688 cm^{-1} due to the vibration of the extension of the OH bond of the hydrated water molecule of the gypsum. The peaks observed at 3382 cm^{-1} and 1621 cm^{-1} correspond to vibrational

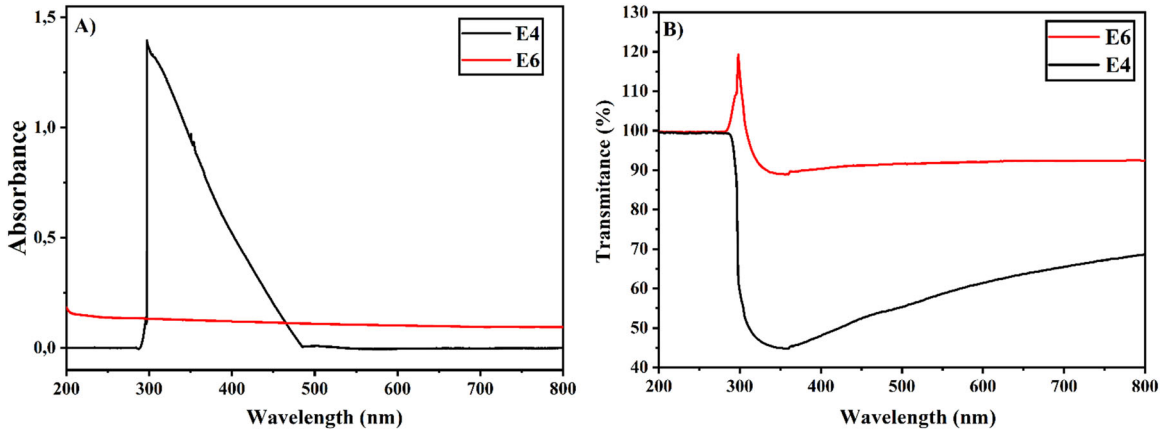

Figure 3. Transmittance (A) and absorbance (B) spectra of solid residue of PG (50%) + Fe (50%) (E4) mixture after acid attack and solid residue after acid attack on raw PG (E6).

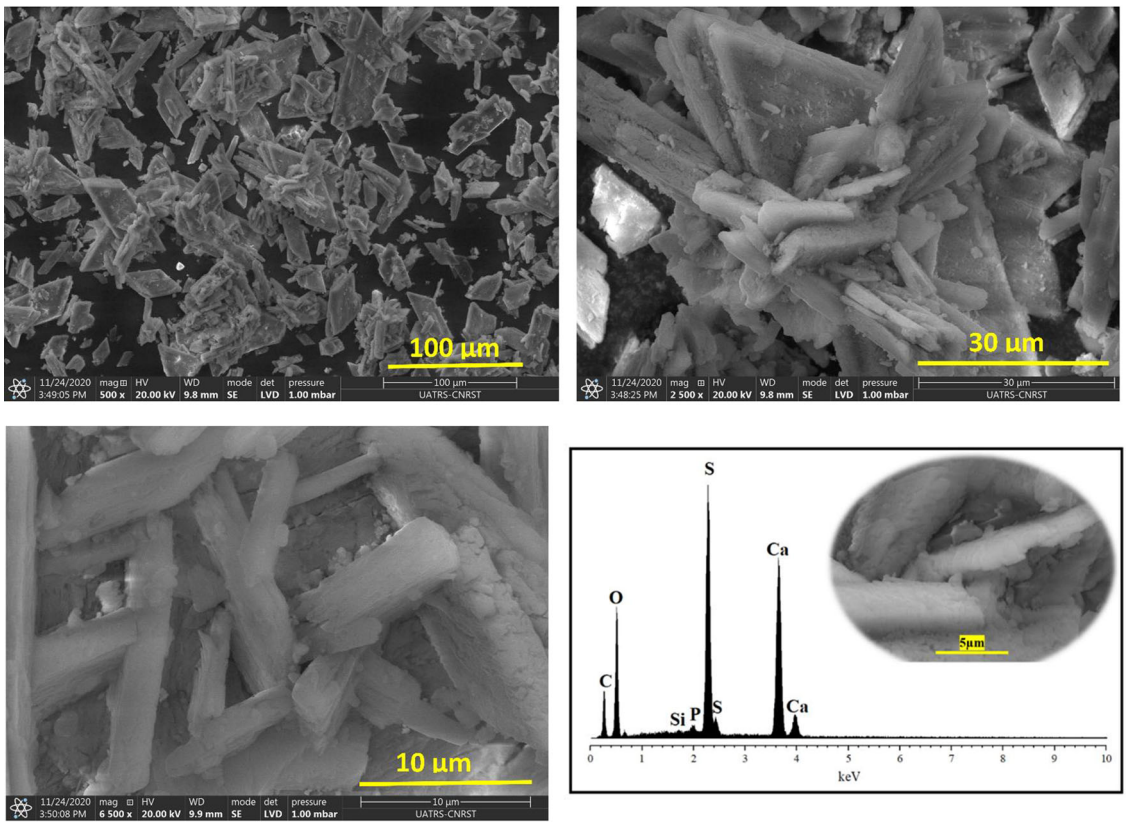

Figure 4. SEM images and EDX spectrum of raw PG.

elongation of OH group of physiosorbed water and the deformation vibration of OH bond, respectively.[49] The appearance of the peak at 1152 cm^{-1} is likely due to vibrational deformation of Fe-OH bond.[50] The occurrence of two peaks at 3218 and 3180 cm^{-1} is attributed to the vibration of the extension of the P-OH bond of residual P_2O_5 in PG. The characteristic peaks of CaS are in excess of the medium infrared region, so the FTIR analyzer fails to give the entire spectrum of CaS.[51] However, the small peak observed at 801 cm^{-1} can be attributed to the deformation of the Ca-S bond in CaS [40] or to symmetrical stretching vibration of $Si-O$.[52,53] The peaks situated at 663 and 591 cm^{-1} are assigned to the asymmetric O-P-O bending ($\nu 4$) of acidic phosphate ions (HPO_4^{2-}) impurities.[51,54]

The UV-Visible spectra of the solid residue, obtained by HCl attack of the PG alone or in the presence of iron, are illustrated in Figure 3. With the presence of Fe, the solid residue have an absorbance between 200 and 500 nm in the UV-Visible region. Optimum photoluminescence occurs at 298 nm, this value is consistent with that given by Barrett et al.[55] Pure CaS shows a strong peak around 220 nm with a small shoulder at 250 nm.[56] CaS sample, prepared by mixing $Ca(CH_3CO_2)_2$ and Na_2S, shows absorbance peak at 405 nm.[57] Natural calcium sulfide (CaS) or oldhamite, from meteorites, is phosphorescent like laboratory-produced compounds. Oldhamite has a high reflectance in the ultraviolet and a weak inflections or shoulders near 360 nm and 375 nm.[58]

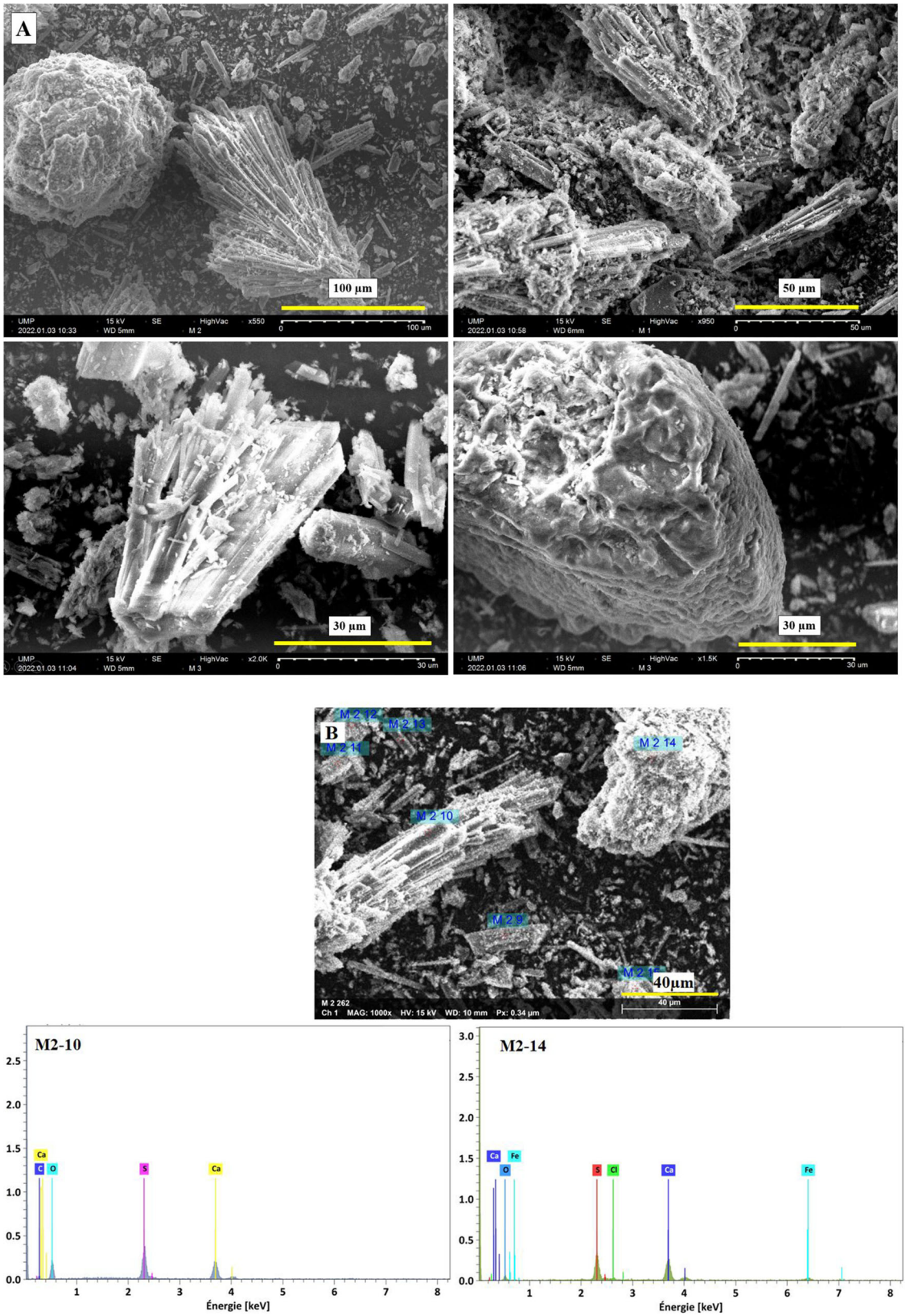

Figure 5. SEM images (A) and EDX spectra (B) of different grain forms of residue. M2-14: Rounded grains; M2-12: Agglomerated needles.

While, PG alone do not shows any absorbance in the UV-Visible region (Figure 3A). The absorbance between 200 and 500 nm is of low intensity and due to the presence of CaS in solid residue.[55–58] This low intensity is due to the fact that calcium sulfide is unstable in water, and requires special precautions during preparation and storage. It will hydrolyze to form hydrates and easily dissolves in an acid solution.

In transmittance mode (Figure 3B), the solid residue of PG (50%) + Fe (50%) sample shows an extinction of 56%

Table 2. Chemical composition (EDX) of residue.

Element	Mass (%)	Standardized mass (%)	Atom (%)	Atomic ratio
Agglomerated needles (M2 10)				
C	5.47	10.9	16.81	
O	29.2	58.19	67.33	O/(S + Ca) = 4.24
S	6.89	13.73	7.93	
Ca	8.61	17.17	7.93	Ca/S = 1.00
Rounded grains (M2 14)				
O	8.59	29.41	50.94	O/(S + Ca) = 1.29
S	5.77	19.77	17.08	
Cl	0.44	1.51	1.18	
Ca	9.46	32.42	22.41	Ca/S = 1.31
Fe	4.93	16.9	8.39	Fe/Cl = 7.11

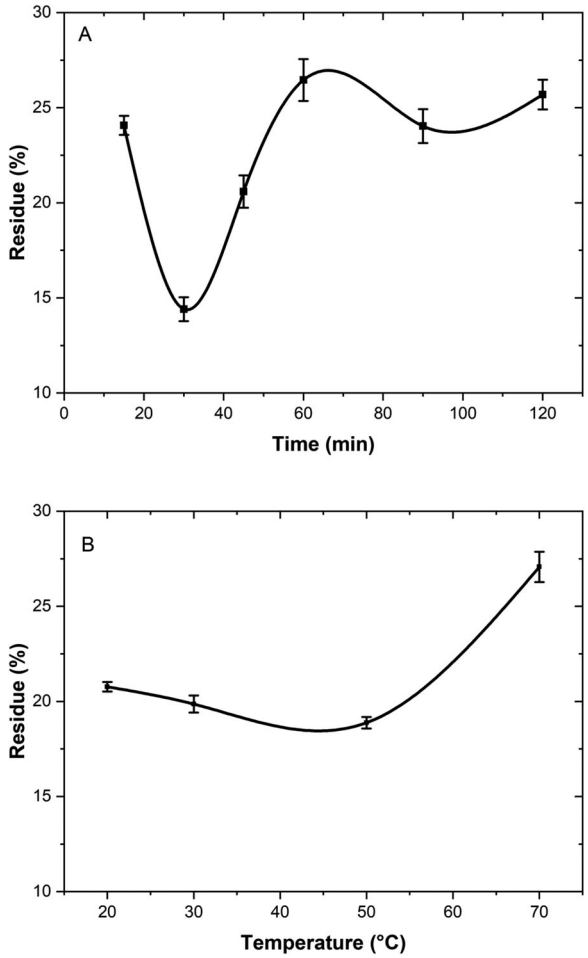

Figure 6. Impact of A) time (min) and B) temperature (°C) on acidic decomposition of PG mixed with Fe metallic.

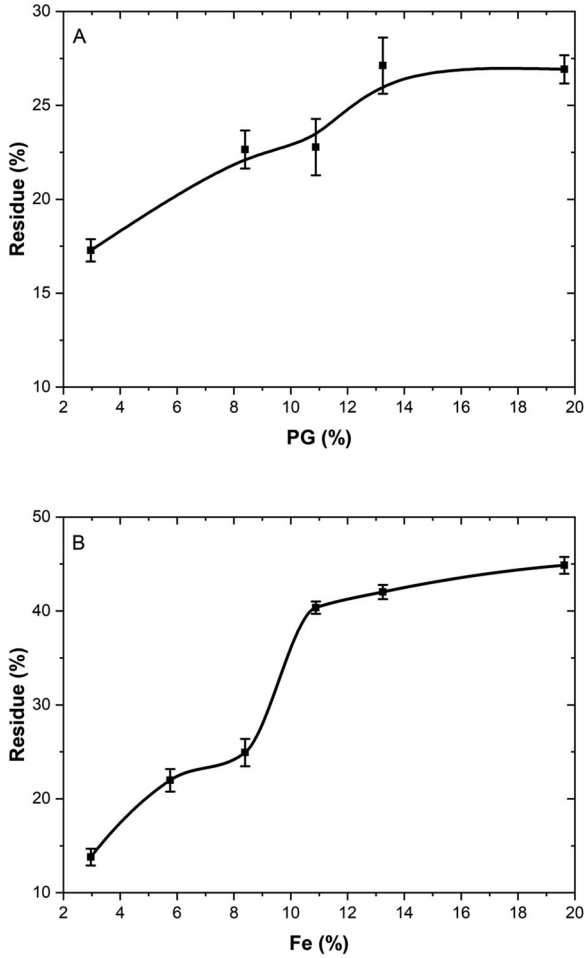

Figure 7. Impact of the amounts of PG (A) and Fe (B) added.

from 280 nm. While the extinction is less than 10% for PG attacked by HCl. CaS has a low absorbance ranging from 0 to 0.17, high transmittance ranging from 70 to 100% and low reflectance ranging from 0 to 15% in the ultraviolet.[59] In transmittance mode, by comparing the two products attacked by HCl, we confirm the presence of CaS, which is an excellent phosphor host material.

SEM images show that the micromorphology of PG is in the form of needles (Figure 4). In addition, the crystals of PG are thin, long and overlap to form aggregates.[60] EDX analysis shows that PG consists mainly of Ca and S with low P and Si contents. The presence of P is due to the presence of a small amount of phosphoric acid. While, the presence of Si is due to the presence of quartz from the phosphate bedrock.

After hydrochloric leaching of PG in the presence of iron, two grain forms are present in the residue: rounded grains (M2 10) and agglomerated needles (M2 14) (Figures 5). Calcium sulfate grains, whose the surface is altered, are in the form of agglomerated needles. The rounded grains have a diameter greater than 100 µm. The EDX results (Table 1) of agglomerated needles give Ca/S = 1.00 and O/(S + Ca) = 4.24, which is close to 4 for the agglomerates of gypsum crystals whose anhydrous formula is $CaSO_4$. Furthermore, the Ca/S and O/(S + Ca) ratios of rounded grains are respectively equal to 1.31 and 1.29. The high concentration of calcium on the surface of the grains can be due to the oxidation of CaS and CaO or by adsorption of OH^- ions on the surface of the grains by Vander Walls type bonds with Ca^{2+} cations. Indeed, H_2O molecules activate the decomposition of CaS into CaO.[61] In an environment where oxygen gas is scant, CaS can transform into CaO and SO_2.[62]

EDX results show the presence of iron and chlorine in small quantities on the surface of the rounded grains (Figure 5). XRD revealed the formation of $FeCl_2.4H_2O$ in the formed residues. The Fe/Cl ratio obtained by EDX is equal to 7 (Table 2), which suggests that there are traces of metallic iron and ferrous chlorides.

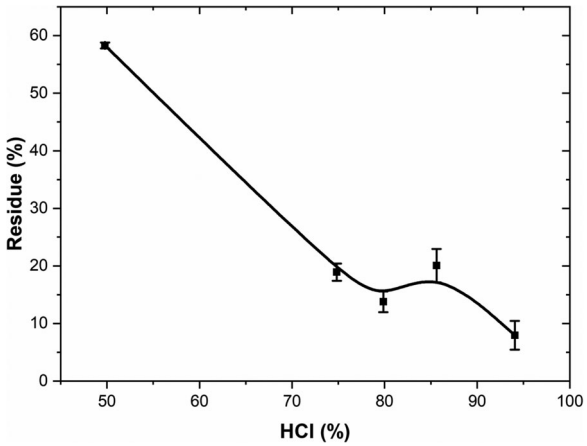

Figure 8. The influence of hydrochloric acid on decomposition of phosphogypsum.

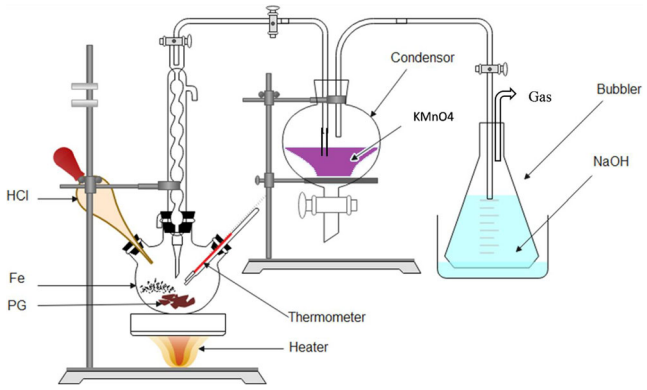

Figure 9. Schematic overview of the experimental design.

Experimental procedures of decomposition of PG

Impact of temperature and time on reactions of decomposition. Figure 6a gives the evolution of the loss of mass of a mixture (mPG = 3 g, mFe = 3 g, VHCl = 25 mL, time = 30 min) as a function of temperature. The loss of mass is very important; it reaches its maximum at 50 °C, which corresponds to the temperature of maximum solubility of gypsum in water.[63]

The evolution of the loss of mass of the mixture (mPG = 3 g, mFe = 3 g, VHCl = 25 mL, T = 50 °C) as a function of time (Figure 6A) shows a maximum loss of 85% after 30 min of attack followed by a stabilization at 75% after 60 min. This stabilization can be explained by the recrystallization of $FeCl_2.4H_2O$ due to the evaporation of water after a long time at 50 °C. Indeed, the solubility of $FeCl_2.4H_2O$ in water is very high in the range of 1600 g/L at 10 °C and reaches 4100 g/L at 100 °C. In our case, the addition of 3 g of Fe in 25 mL of HCl (12.06 M), the maximum concentration of $FeCl_2.4H_2O$ is 2143 g/L, which is at the limit of supersaturation.

Impact of the amounts of PG and Fe-catalysis on decomposition. When the amounts of PG (mFe = 3 g, VHCl = 25 mL, T = 50 °C, Time = 30 min) or that of Fe (mPG = 3 g, VHCl = 25 mL, T = 50 °C, Time = 30 min) increases, the loss of mass decreases (Figure 7). For PG, the reduction in mass loss is not significant, compared to that obtained by adding Fe. The influence of the amount of PG added is small because it decomposes to give SO_2 gas, probably H_2S that leaves the reaction medium. The addition of iron allows the formation of the $FeCl_2.4H_2O$ salt.

Impact of acid volume. By varying the volume of the acid (mPG = 3 g, mFe = 3 g, Temperature = 50 °C, Time = 30 min), the loss increases sharply from 5 to 10 mL of HCl added (Figure 8). This is probably due to the strong evaporation of HCl, which represents 37% by mass of acid volume. The mass loss stabilizes at 85% when the added HCl content is very high. The saturated vapor of concentrated hydrochloric acid solution (> 12 M) contains more than 72% of HCl at 50 °C. This amount of volatile gas increased exponentially at high temperatures.[64]

Conclusion

The decomposition of phosphogypsum by hydrochloric attack and metallic iron catalysis was studied. The solid residue obtained has been determined and monitored. In addition, the impact of experimental parameters as temperature, attack time, mass of iron and PG and volume of acid on PG decomposition were discussed.

Almost complete acid digestion, with concentrated HCl, of PG mixed with iron gave a solid residue consisting of CaS, anhydrite, bassanite and ferrous chloride. The formation of CaS is highlighted by XRD and confirmed by UV-Visible spectroscopy in transmittance and absorbance mode. The decomposition of PG is influenced by temperature, with a maximum decomposition is obtained at 40-50 °C corresponding to the maximum solubility of gypsum. Likewise, time affects decomposition of PG that reaches the maximum after 30 min of attack.

The amount of insoluble solid residue increase as the amounts of PG or Fe increases. This increase is more noticeable for iron, allowing the formation of $FeCl_2.4H_2O$ solid, as evidenced by XRD. The increase of the volume of very volatile HCl stabilizes the amount of the solid residue obtained at around 10%. While, the addition of less than 32 wt.% of HCl gives only CaS. This suggests the development of other reactions allowing the formation of volatile compounds such as SO_2.

Experimental

Raw material

The phosphogypsum studied is from the Chérifien Office of Phosphates of the Jorf Lasfar (El Jadida, Morocco). We used powdered metallic iron (Fe) as a catalyst. The concentration of hydrochloric acid used is 12.06 M. Concentrated HCl 36 M is used to compensate any loss during evaporation of this acid.

Experimental procedures

The PG, having a particle size of less than 250 μm, was dried in an oven at 50 °C for 12 h, and was mixed in a thermostatic flask with metallic iron (Table 1). The flask, linked to

a distillation column, is connected to a condenser, which bubbles the gas leaving in a solution of $KMnO_4$ (0.02 M) the gas continues its way to another bubbler containing a solution of NaOH (0.1 N). The excess gas, escaping from the second bubbler, is tested by a paper impregnated with a solution of $KMnO_4$ (Figure 9).[38]

The temperature was varied from 20 to 70 °C, the mass of PG from 1 to 5 g, the degradation time from 15 to 120 min, the mass of Fe from 1 to 5 g and the volume of HCl from 5 to 30 mL. The solid residues were collected, dried in an oven at 110 °C for 24 h and then weighed. The weight ratio of the insoluble solid residue relative to the initial mass placed in the reactor ($m_{PG} + m_{Fe} + m_{HCl}$) was determined.

Characterization techniques

The X-ray diffraction was carried out on fine crushed powder by a Shimadzu XRD 6100 diffractometer equipped with a Cu X-ray tube (Faculty of sciences, Oujda, Morocco), operating at 40 kV and 30 mA, in the range 2°–70° 2θ. The Attenuated Total Reflection-Fourier Transform Infrared (ATR-FTIR) analysis was obtained using a Fourier transform spectrometer (FT/IR-4700, JASCO), equipped with a DLaTGS detector and Peltier temperature control (Faculty of sciences, Oujda, Morocco). Rapid 10 Hz scan with a resolution of 0.4 cm^{-1} have acquired in a wavelength range of 400–4000 cm^{-1}. Powdered samples were mixed with KBr before analysis. UV-Visible spectroscopy was performed by a Jasco V-730 double beam UV/visible spectrophotometer in the range of 200-800 nm (Faculty of Sciences, Oujda, Morocco). The spectra were recorded on diluted aqueous suspensions obtained by ultrasonic agitation. The scanning electron microscope (SEM) equipped with energy-dispersive X-ray detectors (EDX), Quanta 200 model, was used to observe microstructure of samples studied.

ORCID

El Khadir Gharibi http://orcid.org/0000-0001-8036-5242

References

[1] Ghisellini, P.; Cialani, C.; Ulgiati, S. A Review on Circular Economy: The Expected Transition to a Balanced Interplay of Environmental and Economic Systems. *J. Cleaner Prod.* **2016**, *114*, 11–32. DOI: 10.1016/j.jclepro.2015.09.007.

[2] Luhar, S.; Cheng, T.-W.; Nicolaides, D.; Luhar, I.; Panias, D.; Sakkas, K. Valorisation of Glass Waste for Development of Geopolymer Composites–Mechanical Properties and Rheological Characteristics: A Review. *Constr. Build. Mater.* **2019**, *220*, 547–564. DOI: 10.1016/j.conbuildmat.2019.06.041.

[3] Tayibi, H.; Choura, M.; López, F.-A.; Alguacil, F.-J.; López-Delgado, A. Environmental Impact and Management of Phosphogypsum. *J. Environ. Manage.* **2009**, *90*, 2377–2386. DOI: 10.1016/j.jenvman.2009.03.007.

[4] Oumnih, S.; Gharibi, E.; Yousfi, E.-B.; Bekkouch, N.; El Hammouti, K. Posphogypsum Waste Valorization by Acid Attack with the Presence of Metallic Iron. *J. Mater. Environ. Sci.* **2017**, *8*, 338–344.

[5] Tsioka, M.; Voudrias, E.-A. Comparison of Alternative Management Methods for Phosphogypsum Waste Using Life Cycle Analysis. *J. Cleaner. Prod.* **2020**, *266*, 121386. 2020 DOI: 10.1016/j.jclepro.2020.121386.

[6] Ennaciri, Y.; Bettach, M.; Cherrat, A.; Zegzouti, A. Conversion of Phosphogypsum to Sodium Sulfate and Calcium Carbonate in Aqueous Solution. *J. Mater. Environ. Sci.* **2016**, *7*, 1925–1933.

[7] De Ridder, M.; De Jong, S.; Polchar, J.; Lingemann, S. The Hague Centre for Strategic Studies (HCSS). Rapport N° 17 | 12 | 12 ISBN/EAN: 978-94-91040-69-6, **2012**.

[8] Mar, S.-S.; Okazaki, M. Investigation of Cd Contents in Several Phosphate Rocks Used for the Production of Fertilizer. *Microchem. J.* **2012**, *104*, 17–21. DOI: 10.1016/j.microc.2012.03.020.

[9] U.S. Geological Survey, Mineral commodity summaries 2012: U.S. Geological Survey, **2012**, 198 p.

[10] Cooper, J.; Lombardi, R.; Boardman, D.; Carliell-Marquet, C. The Future Distribution and Production of Global Phosphate Rock Reserves. *Resour. Conserv. Recycl.* **2011**, *57*, 78–86. DOI: 10.1016/j.resconrec.2011.09.009.

[11] Walan, P.; Davidsson, S.; Johansson, S.; Höök, M. Phosphate Rock Production and Depletion: Regional Disaggregated Modeling and Global Implications. *Resour., Conserv. Recycl.* **2014**, *93*, 178–187. DOI: 10.1016/j.resconrec.2014.10.011.

[12] Hammas, I.; Horchani-Naifer, K.; Férid, M. Solubility Study and Valorization of Phosphogypsum Salt Solution. *Inter. J. Miner. Process.* **2013**, *123*, 87–93. DOI: 10.1016/j.minpro.2013.05.008.

[13] Amrani, M.; Taha, Y.; Kchikach, A.; Benzaazoua, M.; Hakkou, R. Recycling: New Horizons for a More Sustainable Road Material Application. *J. Build. Eng.* **2020**, *30*, 101267. DOI: 10.1016/j.jobe.2020.101267.

[14] Chernysh, Y.; Yakhnenko, O.; Chubur, V.; Roubík, H. Phosphogypsum Recycling: A Review of Environmental Issues, Current Trends, and Prospects. *Appl. Sci.* **2021**, *11*, 1575. DOI: 10.3390/app11041575.

[15] Geraldo, R.-H.; Costa, A.-R.-D.; Kanai, J.; Silva, J.-S.; Souza, J.-D.; Andrade, H.-M.-C.; Gonçalves, J.-P.; Fontanini, P.-S.-P.; Camarini, G. Calcination Parameters on Phosphogypsum Waste Recycling. *Constr. Build. Mater.* **2020**, *256*, 119406. DOI: 10.1016/j.conbuildmat.2020.119406.

[16] Wu, S.; Yao, X.; Ren, C.; Yao, Y.; Wang, W. Recycling Phosphogypsum as a Sole Calcium Oxide Source in Calcium Sulfoaluminate Cement and Its Environmental Effects. *J. Environ. Manage.* **2020**, *271*, 110986. DOI: 10.1016/j.jenvman.2020.110986.

[17] Sfar Felfoul, H.; Clastres, P.; Carles-Gibergues, A.; Ben Ouezdou, M. Propriétés et Perspectives D'utilisation du Phosphogypse. L'exemple de la Tunisie. *Cim., Bétons, Plâtres, Chaux* **2001**, *849*, 186–191.

[18] Murat, M.; Sorrentino, F. Effect of Large Additions of Cd, Pb, Cr, Zn, to Cement Raw Meal on the Composition and the Properties of the Clinker and the Cement. *Cem. Concr. Res.* **1996**, *26*, 377–385. DOI: 10.1016/S0008-8846(96)85025-3.

[19] Silva, M.-V.; de Rezende, L.-R.; dos Anjos Mascarenha, M.-M.; de Oliveira, R.-B. Phosphogypsum, Tropical Soil and Cement Mixtures for Asphalt Pavements under Wet and Dry Environmental Conditions. *Resour. Conserv. Recycl.* **2019**, *144*, 123–136. DOI: 10.1016/j.resconrec.2019.01.029.

[20] de Rezende, L.-R.; Curado, T.-D.-S.; Silva, M.-V.; Mascarenha, M.-M.-D.-A.; Metogo, D.-A.-N.; Neto, M.-P.-C.; Bernucci, L.-L.-B. Laboratory Study of Phosphogypsum, Stabilizers, and Tropical Soil Mixtures. *J. Mater. Civ. Eng.* **2017**, *29*, 04016188. DOI: 10.1061/(ASCE)MT.1943-5533.0001711.

[21] Zeng, L.-L.; Bian, X.; Zhao, L.; Wang, Y.-J.; Hong, Z.-S. Effect of Phosphogypsum on Physiochemical and Mechanical Behaviour of Cement Stabilized Dredged Soil from Fuzhou. *China. Geomech. Energy Environ.* **2021**, *25*, 100195. DOI: 10.1016/j.gete.2020.100195.

[22] Oumnih, S.; Bekkouch, N.; Gharibi, E.-K.; Fagel, N.; Elhamouti, K.; El Ouahabi, M. Phosphogypsum Waste as Additives to Lime Stabilization of Bentonite. *Sustainable Environ. Res.* **2019**, *29*, 1–10. DOI: 10.1186/s42834-019-0038-z.

[23] Harrou, A.; Gharibi, E.-K.; Taha, Y.; Fagel, N.; El Ouahabi, M. Phosphogypsum and Black Steel Slag as Additives for Ecological Bentonite-Based Materials: Microstructure and Characterization. *Minerals* **2020**, *10*, 1067. DOI: 10.3390/min10121067.

[24] Rutherford, P.-M.; Dudas, M.-J.; Arocena, J.-M. Trace Elements and Fluoride in Phosphogypsum Leachates. *Environ. Technol.* **1995**, *16*, 343–354. DOI: 10.1080/09593331608616276.

[25] Romero-Hermida, M.-I.; Flores-Alés, V.; Hurtado-Bermúdez, S.-J.; Santos, A.; Esquivias, L. Environmental Impact of Phosphogypsum-Derived Building Materials. *Int. J. Environ. Res. Public Health* **2020**, *17*, 4248.*ijerph* DOI: 10.3390/17124248.

[26] Xu, P.; Li, H.; Chen, Y. Experimental Study on Optimization of Phosphogypsum Suspension Decomposition Conditions under Double Catalysis. *Materials* **2021**, *14*, 1120. DOI: 10.3390/ma14051120.

[27] Miao, Z.; Yang, H.; Wu, Y.; Zhang, H.; Zhang, X. Experimental studies on decomposing properties of desulfurization gypsum in a thermogravimetric analyzer and multiatmosphere fluidized beds. *Ind. Eng. Chem. Res.* **2012**, *51*(15), 5419–5423 DOI: 10.1021/ie300092s.

[28] Bhawan, P.; Nagar, E.-A. Hazardous Waste Management. Ministry of Environment & Forests: Delhi, **2012**.

[29] Marty, M. Analyses-diagnostics du potentiel de résilience d'une organisation. Doctoral Dissertation. École Polytechnique de Montréal, **2014**.

[30] Wheelock, T.-D.; Boylan, D.-R. Reductive Decomposition of Gypsum by Carbon Monoxide. *Ind. Eng. Chem.* **1960**, *52*, 215–218. DOI: 10.1021/ie50603a023.

[31] Zheng, M.; Shen, L.; Feng, X.; Xiao, J. Kinetic Model for Parallel Reactions of $CaSO_4$ with CO in Chemical-Looping Combustion. *Ind. Eng. Chem. Res.* **2011**, *50*, 5414–5427. DOI: 10.1021/ie102252z.

[32] Kühle, K.-D.; Knösel, K.-R. Process for the production of cement clinker and waste gases containing sulphur dioxide éd: Google Patents, **1988**.

[33] Yan, B.; Ma, L.; Ma, J.; Zi, Z.; Yan, X. Mechanism Analysis of Ca, S Transformation in Phosphogypsum Decomposition with Fe Catalyst. *Ind. Eng. Chem. Res.* **2014**, *53*, 7648–7654. DOI: 10.1021/ie501159y.

[34] Wheelock, T.-D. Simultaneous Reductive and Oxidative Decomposition of Calcium Sulfate in the Same Fluidized Bed. U.S. Patent No. 4,102,989. Washington, DC: U.S. Patent and Trademark Office. **1978**.

[35] Smith, L.-L.; Fortney, M.-L.; Morris, C.-E.; Wheelock, T.-D.; Carrazza, J.-A. Resource Recovery from Wastewater Treatment Sludge Containing Gypsum. In *Eleventh National Waste Processing Conference and Exhibit*, **1984**, p. 19.

[36] Nengovhela, R.-N. The Recovery of Sulphur from Waste Gypsum. Doctoral Dissertation, University of Pretoria, Pretoria, **2009**.

[37] Aagli, A.; Tamer, N.; Atbir, A.; Boukbir, L.; El Hadek, M. Conversion of Phosphogypsum to Potassium Sulfate: Part I. The Effect of Temperature on the Solubility of Calcium Sulfate in Concentrated Aqueous Chloride Solutions. *J. Therm. Anal. Calorim.* **2005**, *82*, 395–399. DOI: 10.1007/s10973-005-0908-y.

[38] Oumnih, S. Étude de valorisation du phosphogypse par désulfuration et par ajout à la stabilisation des sols gonflants. Doctoral Dissertation, Université Mohammed Premier, Oujda, Maroc and Université de Liège, Liege, Belgique, **2020**.

[39] Wu, S.-Y.-H.; Tseng, C.-L.; Lin, F.-H. A Newly Developed Fe-Doped Calcium Sulfide Nanoparticles with Magnetic Property for Cancer Hyperthermia. *J. Nanopart Res.* **2010**, *12*, 1173–1185. DOI: 10.1007/s11051-009-9734-7.

[40] Allen, D.; Hayhurst, A.-N. Reaction between Gaseous Sulfur Dioxide and Solid Calcium Oxide Mechanism and Kinetics. *Faraday Trans.* **1996**, *92*, 1227–1238. DOI: 10.1039/ft9969201227.

[41] Shobhana, E. Optical Characterization of Calcium Sulphide (CaS) Thin Films by Chemical Bath Deposition. *Int. J. Sci. Res.* **2015**, *4*, 1696–1701.

[42] Wu, S.-Y.-H.; Yang, K.-C.; Tseng, C.-L.; Chen, J.-C.; Lin, F.-H. Silica-Modified Fe-Doped Calcium Sulfide Nanoparticles for in Vitro and in Vivo Cancer Hyperthermia. *J. Nanopart Res.* **2011**, *13*, 1139–1149. DOI: 10.1007/s11051-010-0106-0.

[43] Louvain, N.; Fakhry, A.; Bonnet, P.; El-Ghozzi, M.; Guérin, K.; Sougrati, M.-T.; Jumas, J.-C.; Willmann, P. One-Shot versus Stepwise Gas–Solid Synthesis of Iron Trifluoride: Investigation of Pure Molecular F_2 Fluorination of Chloride Precursors. *CrystEngComm* **2013**, *15*, 3664–3671. DOI: 10.1039/c3ce27033e.

[44] Sürer, M.-G.; Arat, H.-T. State of Art of Hydrogen Usage as a Fuel on Aviation. *Eur. Mech. Sci.* **2017**, *2*, 20–30. DOI: 10.26701/ems.364286.

[45] Odom, J.-M. Industrial and Environmental Activities of Sulfate-Reducing Bacteria. In *The Sulfate-Reducing Bacteria: Contemporary Perspectives*. New York: Springer-Verlag, **1993**. pp. 189–210.

[46] Gou, Z.; Chang, J.; Gao, J.; Wang, Z. In Vitro Bioactivity and Dissolution of $Ca_2(SiO_3)(OH)_2$ and β-Ca_2SiO_4 Fibers. *J. Eur. Ceram. Soc.* **2004**, *24*, 3491–3497. DOI: 10.1016/j.jeurceramsoc.2003.11.023.

[47] Petrosyan, A.-M.; Ghazaryan, V.-V.; Fleck, M. On the Infrared Spectrum of L-Lysinium (2+) Sulfate. *Spectrochim. Acta A Mol. Biomol. Spectrosc.* **2011**, *79*, 2020–2022. DOI: 10.1016/j.saa.2011.04.077

[48] Kugel, R.; Taube, H. Infrared Spectrum and Structure of Matrix-Isolated Sulfur Tetroxide. *J. Phys. Chem.* **1975**, *79*, 2130–2135. DOI: 10.1021/j100587a014.

[49] Naushad, M. Surfactant Assisted Nano-Composite Cation Exchanger: Development, Characterization and Applications for the Removal of Toxic Pb2+ from Aqueous Medium. *Chem. Eng. J.* **2014**, *235*, 100–108. DOI: 10.1016/j.cej.2013.09.013.

[50] Zhang, G.; Qu, J.; Liu, H.; Liu, R.; Wu, R. Preparation and Evaluation of a Novel Fe-Mn binary oxide adsorbent for effective arsenite removal. *Water Res.* **2007**, *41*, 1921–1928. DOI: 10.1016/j.watres.2007.02.009.

[51] Qi, Z.; Wang, Y.; He, H.; Li, D.; Xu, X. Wettability Alteration of the Quartz Surface in the Presence of Metal Cations. *Energy Fuels* **2013**, *27*, 7354–7359. DOI: 10.1021/ef401928c.

[52] Athinarayanan, J.; Jaafari, S.-A.-A.-H.; Periasamy, V.-S.; Almanaa, T.-N.-A.; Alshatwi, A.-A. Fabrication of Biogenic Silica Nanostructures from Sorghum bicolor Leaves for Food Industry Applications. *Silicon* **2020**, *12*, 2829–2836. DOI: 10.1007/s12633-020-00379-4.

[53] Corno, M.; Busco, C.; Civalleri, B.; Ugliengo, P. Periodic ab Initio Study of Structural and Vibrational Features of Hexagonal Hydroxyapatite $Ca_{10}(PO_4)6(OH)2$. *Phys. Chem. Chem. Phys.* **2006**, *8*, 2464–2472. DOI: 10.1039/B602419J.

[54] Ulian, G.; Valdrè, G.; Corno, M.; Ugliengo, P. The Vibrational Features of Hydroxylapatite and Type a Carbonated Apatite: A First Principle Contribution. *Amer. Miner.* **2013**, *98*, 752–759. DOI: 10.2138/am.2013.4315.

[55] Barrett, E.; Fern, G.-R.; Ray, B.; Withnall, R.; Silver, J. UV Photoluminescence from Small Particles of Calcium Cadmium Sulfide Solid Solutions. *J. Opt. A: Pure Appl. Opt.* **2005**, *7*, S265–S269. DOI: 10.1088/1464-4258/7/6/002.

[56] Sharma, G.; Patil, K.-R.; Gosavi, S.-W. Synthesis and Luminescence of Graphene-Nano Calcium Sulphide Composite. *Mater. Chem. Phys.* **2014**, *147*, 57–64. DOI: 10.1016/j.matchemphys.2014.04.006.

[57] Castro, M. E.; Rivera, D. U.S. Patent No. 8,945,494. Washington, DC: U.S. Patent and Trademark Office. **2015**.

[58] Izawa, M.-R.-M.; Applin, D.-M.; Mann, P.; Craig, M.-A.; Cloutis, E.-A.; Helbert, J.; Maturilli, A. Reflectance Spectroscopy (200–2500 nm) of Highly-Reduced Phases under Oxygen-and Water-Free Conditions. *Icarus* **2013**, *226*, 1612–1617. DOI: 10.1016/j.icarus.2013.08.014.

[59] Nnabuchi, M.-N.; Okeke, C.-E. Characterization of Optimized Grown Calcium Sulphide Thin Films and Their Possible Applications in Solar Energy. *Pac. J. Sci. Technol.* **2004**, *5*, 72–82.

[60] Li, H.; Zhang, H.; Li, L.; Ren, Q.; Yang, X.; Jiang, Z.; Zhang, Z. Utilization of Low-Quality Desulfurized Ash from Semi-Dry Flue Gas Desulfurization by Mixing with Hemihydrate Gypsum. *Fuel* **2019**, *255*, 115783. DOI: 10.1016/j.fuel.2019.115783.

[61] Wu, S.; Uddin, M.-A.; Nagamine, S.; Sasaoka, E. Role of Water Vapor in Oxidative Decomposition of Calcium Sulfide. *Fuel* **2004**, *83*, 671–677. DOI: 10.1016/j.fuel.2003.10.027.

[62] Song, Z.; Zhang, M.; Ma, C. Study on the Oxidation of Calcium Sulfide Using TGA and FTIR. *Fuel Process. Technol.* **2007**, *88*, 569–575. DOI: 10.1016/j.fuproc.2007.01.014.

[63] Seidel, G.; Huckauf, H.; Stark, J. *Technologie des ciments, chaux, plâtre: Processus et installations de cuisson*. Éditions SEPTIMA, **1980**

[64] EPA. Toxic Release Inventory. U.S. Environmental Protection Agency: Washington, **1995.**